

Removal of Gallic Acid Over Layered Double Hydroxide: Material Design and Kinetic Studies

Abdelmadjid Chedri Mammam^{1,2}, Hanene Zazoua¹, Souhila Ait Hamoudi¹, Dalila Hadiouche³, Lotfi Mouni³ , Khaldoun Bachari¹ , Amel Boudjemaa^{1,*} 

¹ Scientific and Technical Research Center in Physico-chemical Analysis (CRAPC), BP 384, Bou-Ismaïl, RP 42004, Tipaza, Algeria. chedri_ma@yahoo.fr (A.M); hanene_zazoua@yahoo.fr (H.Z.); souh_ait@yahoo.fr (S.A.); amel_boudjemaa@yahoo.fr (A.B); bachari2000@yahoo.fr (K.B.);

² Laboratory of the Management and Development of Natural Resources and Quality Assurance SNVST Faculty, University of Akli Mohand Oulhadj, Bouira, Algeria. dalila.hadiouche@gmail.com (D.H), lotfimouni@gmail.com (L.M.);

* Correspondence: amel_boudjemaa@yahoo.fr; amel.boudjemaa@crapc.dz (A.B.);

Scopus Author ID 24740996500

Received: 25.07.2022; Accepted: 24.11.2022; Published: 7.02.2023

Abstract: The present study focused on removing gallic acid on the layered double hydroxide (Mg-Al-LDH) material synthesized by the co-precipitation method with a molar ratio of Mg/Al = 2. The elaborated Mg-Al-LDH was characterized using chemical analysis, XRD, FTIR, SEM, and specific surface area techniques. Langmuir and Freundlich isotherms and kinetic studies were also investigated. The adsorption tests demonstrated that the GA adsorption onto the Mg-Al-LDH is dependent on the material dose, GA concentration, and the pH of the solution. It was observed that the yield of the dye removal passed from 27.37 to 99.9 %; when the Mg-Al-LDH dose increased from 0.05 to 0.8 g/L. The results obtained showed that the adsorption of GA on Mg-Al-LDH is an endothermic reaction, spontaneous, follows second-order kinetics, and the Langmuir isotherm observed a better description.

Keywords: layered double hydroxide; gallic acid; kinetic, thermodynamic, isotherm models.

© 2023 by the authors. This article is an open-access article distributed under the terms and conditions of the Creative Commons Attribution (CC BY) license (<https://creativecommons.org/licenses/by/4.0/>).

1. Introduction

Gallic acid (3,4,5-trihydroxybenzoic acid, GA) is the main phenolic component found in black tea, nutgall, sumac spice, cork oak, grape, and wine, and it is also widely has been used in paints and dyes, medicine, food, and metallurgical industry [1-5]. The presence of GA as a micropollutant in wastewater, even at low concentrations, has toxicities [6], so it can react with chlorine during wastewater treatment to form toxic and even pathogenic halogenated organic compounds, present a potential danger to human life and the environment. It has been shown that excess GA in water causes the unpleasant color and odor of drinking water during the chlorination process due to the formation of carcinogenic disinfection byproducts, such as trichloroethanes and chloroacetic acids [7-9].

The accumulation of GA in the environment should be avoided. In addition, GA in water where presents a very low biodegradability due to its solubility in water and low molecular weight [10,11]. Various techniques have been used to remove GA from water, it has been shown that biosorption techniques have been used for the adsorption of GA, but these techniques can inhibit microbial growth [10]. It has also been shown that Fenton processes, including photo-Fenton and electrochemical Fenton treatment [12,13], have been used for the

degradation of GA, but these processes may give contamination as a result of the intermediates formed.

The adsorption process using different adsorbents has attracted particular interest for removing GA from aqueous systems due to its convenient operation, lower cost, high efficiency, and the reusability of adsorbents. Recently, several types of adsorbents have been used for the removal of GA, such as resins [9], activated carbon [14], biomass [10], clay minerals [15], magnetic nanoparticles [16], clay and polymer systems [17].

Layered double hydroxides (LDHs), also known as hydrotalcite-like compounds [18], belong to a class of anionic clays. The general LDH' formula is $[M^{2+}_{1-x}M^{3+}_x(OH)_2]^{x+} [A^{m-}_{x/m} nH_2O]^{x-}$, where M^{2+} and M^{3+} are divalent and trivalent cations. The x value represents the ratio between M^{3+} and $(M^{2+}+M^{3+})$ ($M^{3+}/(M^{2+}+M^{3+})$), and A^{m-} is a charge-balancing interlayer anion. Generally, x values ranged from 0.10 to 0.33 [19]. These materials exhibit an excellent ability to eliminate organic and inorganic anions due to the presence of positively charged brucite-like sheets, weak interlayer bonding, and ion exchange properties [18, 20]. So, the large surface area, high anion exchange capacity, and good thermal stability of LDHs ensure their application in the environmental field for the removal of organic and inorganic compounds such as surfactants [21], phenolic compounds [22, 23], phosphate [24-27] fluoride, arsenate [28], arsenite [29], chromate [30], selenite and selenite [31], nitrates [32, 33], sulfates [34] chloride [35,36], perchlorate and oxyanions [37].

Recently, hydrotalcite-like compounds have been applied to the removal of GA [38-41]. So, the studies of the adsorption of GA on fresh and calcined Ni-Al layered double hydroxides demonstrated that calcined Ni-Al-LDH could remove more than 94% of GA at 500 °C. The adsorption equilibrium followed the Freundlich model. The process was endothermic, with maximum adsorption capacities of 137.9 and 82.97 mg / g for fresh and calcined Ni-Al-LDH.

The originality and the novelty in this work reside in the choice of adsorbent for the removal of GA. Gallic acid is a phenolic compound in medicinal plants and fruits [42]. It is recovered by extraction [43]. The use of GA and derivatives has gradually increased, thus leading to a further understanding of GA. As well as, GA and ester derivatives as aromatic agents and conservatives are largely used in the food industry [44, 45]. In particular, various ester derivatives are extensively used in the cosmetic industry [46] in transformed and packaged foods to avoid oxidative damage and deterioration; several types of studies were also carried out on the biological and pharmacological activities of GA, including their antioxidants. The antioxidant strength confers its anticancer and antiradical properties. The GA is used to identify different substances' phenolic content [47]. It is thought to possess a wide number of beneficial effects on health and the environment. Mg-Al-LDH was synthesized by the coprecipitation method and characterized by chemical analysis, X-ray Diffraction (XRD), FTIR spectroscopy analysis, surface measurement (N_2 adsorption/desorption), and scanning electron microscopy (SEM) analysis. The reliability of the model equations was analyzed, and the process parameters were optimized, such as the adsorbent amount, adsorption time, and pH of the solution. The possibility of intraparticle diffusion was examined using the Weber-Morris theory. The LDH adsorption capacities were studied via Langmuir and Freundlich isotherms models.

2. Materials and Methods

2.1. Materials.

All used chemicals were of analytical grade and utilized without further purification and were provided by Biochem Chemopharma. All the solutions were prepared by using distilled water, gallic acid (GA: C₇H₆O₅, 99.5%), Folin-Ciocalteu reagent, sodium chloride (NaCl), sodium hydroxide (NaOH), hydrochloric acid (HCl), aluminum nitrate nonahydrate, Al(NO₃)₃·9H₂O, magnesium nitrate hexahydrate Mg(NO₃)₂·6H₂O and anhydrous sodium carbonate (Na₂CO₃).

2.2. Sample preparation.

The Mg-Al-LDH sample with an Mg/Al molar ratio of 2/1 was synthesized by the co-precipitation method [48,49] in the alkaline medium (pH ~10) [50]. An aqueous solution of Mg(NO₃)₂·6H₂O (0.136 mol) and Al(NO₃)₃·9H₂O (0.075 mol) was prepared in distilled water (300 mL). The obtained mixture was added dropwise into a mixture of NaOH (0.6 mol) and NaCO₃ (0.24 mol) under vigorous stirring and at room temperature. After 2 h of stirring, the temperature was increased to 70 °C and maintained for 18 h. The precipitate formed was filtered and washed with hot distilled water until the pH stabilized at 7. Finally, the powder was dried in an oven at 80 °C overnight.

2.3. Characterization techniques.

The chemical composition was determined by atomic absorption Spectrometer 240 FS (Fast Sequential). SEM images were performed on a Quanta 250 instrument with an acceleration voltage of 20 kV and a working distance of 10 mm. X-ray diffraction (XRD) was recorded in the range of 5 –80° on the BRÜKER D8 using Cu K α radiation. The infra-red spectrum (FTIR) was carried out with a Perkin Elmer FTIR 1000 spectrometer; over 32 scans were taken to improve the signal-to-noise ratio in the wavelength range of 400-4000 cm⁻¹. The specific surface area was calculated by the BET method. The pore size distribution curve was obtained from the desorption branch using the BJH method using micrometric ASAP2020 equipment using nitrogen at -196 °C.

2.5 Adsorption studies.

The reaction was carried out at room temperature (25 ± 0.5 °C). 100 mg of Mg-Al-LDH was added to the GA solution (0.1 mg/L) under stirring (180 rpm). The GA concentration, pH, and the adsorbent dose were varied to study their effect on the adsorption kinetics. Using a pH meter, and the solution pH was adjusted with NaOH or HCl (0.1 M). The GA concentration was determined by a UV-Vis spectrophotometer with a double beam (Optizen 3200 spectrophotometer). The adsorption amount at time t, q_t (mg/g), was determined by the following equation:

$$q_t = \frac{C_0 - C_t}{m} \times V \quad (1)$$

C₀ and C_t (mg/L) represent the initial, and the final concentrations, and m is the mass of Mg-Al-LDH (g). The equilibrium amount of adsorption, q_e (mg/g), was determined by the formula:

$$q_e = \frac{C_0 - C_e}{m} \times V \quad (2)$$

C_e (mg/L) is GA concentrations at equilibrium, and the GA removal percentage can be calculated as follows:

$$\text{GA removal (\%)} = \frac{C_o - C_e}{m} \times 100 \quad (3)$$

3. Results and Discussion

3.1. Characterization.

The physicochemical properties of the material are regrouped in Table 1. Mg^{2+}/Al^{3+} and $Al^{3+}/Al^{3+} + Mg^{2+}$ molar ratio is similar to those expected from the initial concentration of the solutions used during the preparation process.

Table 1. The structural and textural properties of the Mg-Al-LDH sample.

Sample	Mg-Al-LDH
Theoretical molar ratio M^{2+}/M^{3+}	2
Real molar ratio M^{2+}/M^{3+}	1.87
$M^{3+} / (M^{2+} + M^{3+})$ molar ratio	0.33
d_{003} (Å)	7.51
a (Å)	3.03
c (Å)	22.53
BET surface area (m^2/g)	75.06
BJH pore volume (cm^3/g)	0.32
BJH pore size (Å)	171.99

The crystalline phase of Mg-Al-LDH is confirmed by XRD (Figure 1), and the peaks show a basal reflection of hydroxalite structure. The diffractogram exhibited the symmetric reflections of (003) and (006) planes in the low values of 2θ ($11-23^\circ$) and asymmetric reflections of (012), (015), and (018) planes at the higher values of 2θ ($34-66^\circ$), characteristic of well crystalline LDH structure [51]. The interlayer spacing calculated from the plane (003) is 7.51 Å confirming the intercalated carbonate anion. The values of unit cell parameters "a" and "c" of Mg-Al-LDH calculated using the formula: $a = 2d_{110}$ and $c = 3d_{003}$ [24,50] where d_{110} and d_{003} are the basal spacing values of (110) and (003) planes, respectively. The "a" cell parameter stands for the cation-cation distance within the brucite-like layer. At the same time, the "a" unit cell parameter is close to that of the natural hydroxalite (3.03 Å) [51]. The parameter "c" gives the combined thickness of the brucite-like layer and the interlamellar space. The value observed for the $c = 22.53\text{Å}$ parameter is typical of LDH containing carbonate as the interlamellar anion [52].

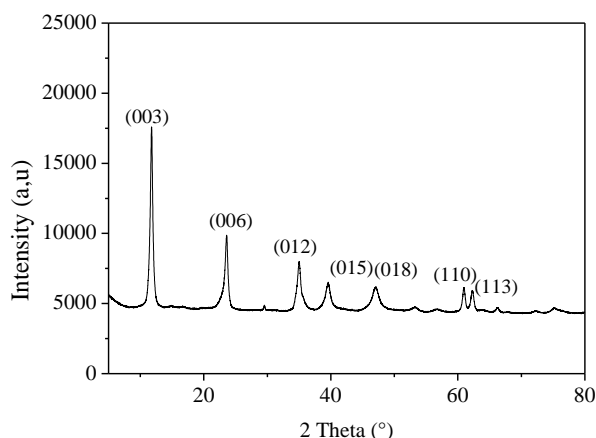


Figure 1. X-ray diffraction of Mg-Al-LDH.

FT-IR spectroscopy analysis can provide useful information about the structure of some materials with a special structure, such as interlamellar anions [53]. The FT-IR spectrum of the Mg-Al-LDH sample is shown in Figure 2. The spectrum shows a wide adsorption band at 3409 cm^{-1} assigned to the OH stretching of the hydroxyl group located in the interlayer space of LDH structure and both adsorbed and interlamellar water [54-56]. The weak band located at 1640 cm^{-1} is attributed to water molecular's HOH deformation mode ($\delta\text{H-O-H}$) [53]. The intense peak at 1354 cm^{-1} is related to the stretching mode of the CO_3^{2-} anion. In the low-frequency region, the bands observed between 1000 and 500 cm^{-1} are characteristic of metal-oxygen-metal vibrations [56]. The textural properties of Mg-Al-LDH are reported in Table 1. It can be seen that the sample has a significant surface area. Based on the IUPCA classification, the values of pore size obtained are characteristic of mesoporous materials [57].

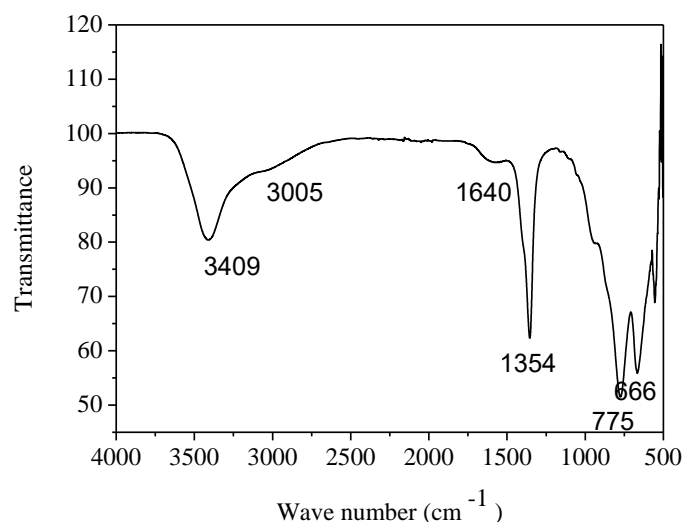


Figure 2. FT-IR spectra of Mg-Al-LDH.

The SEM image in Figure 3 exhibits the presence of microstructure. It is observed that the sample presents lamellar plates that stack parallel to each other due to the strong interaction between particles.

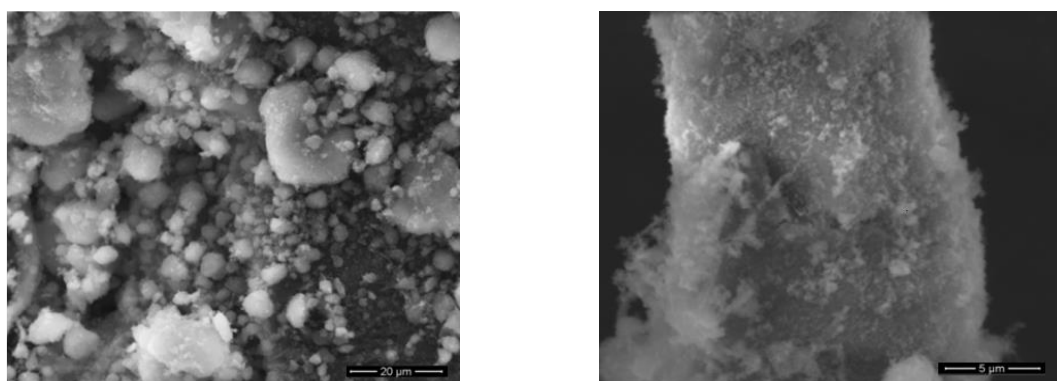


Figure 3. SEM images of Mg-Al-LDH.

3.2. Adsorption studies.

3.2.1. Effect of Mg-Al-HDL dose.

To investigate the Mg-Al-HDL dose effect on the removal efficiency of GA, the adsorbent dose is varied from 0.05 to 0.8 g/L with the initial GA concentration of 0.1 mg/L at 30 °C and pH 4.5. It was observed that the yield of the dye removal passed from 27.37 to 99.9

%; when the Mg-Al-HDL dose increased from 0.05 to 0.8 g/L (Figure 4). This compartment may increase the number of sorption sites with a rise in the mass of Mg-Al-HDL up to a dose of 0.6 g/L; the number of sites becomes stable. A mass < 0.4 g was selected as the optimal adsorbent dosage [58].

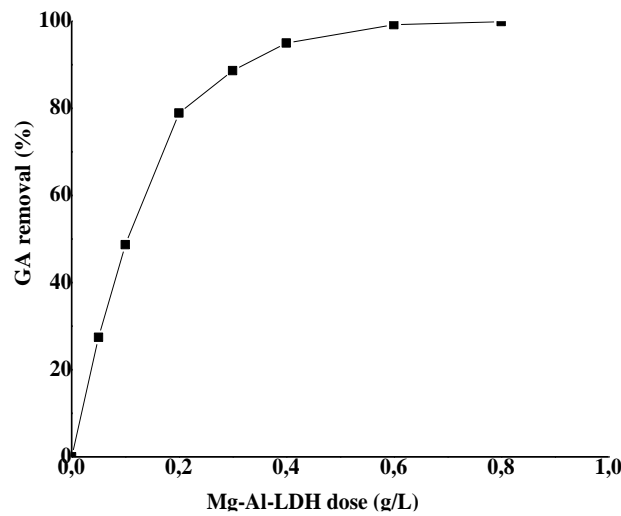


Figure 4. Effect of Mg-Al-LDH amount on the adsorption of GA under conditions: $C_0(\text{GA}) = 0.1 \text{ mg/L}$, reaction time = 360 min, $\text{pH} = 4.5$, $T = 298 \text{ K}$.

3.2.2. Effect of pH.

The solution pH is an important parameter in the adsorption process, particularly for organic compound adsorption. However, the pH also controls the electrostatic charge intensity, which is affected by the ionized species. The surface adsorption capacity and surface active center type are indicated through the significant factor known as the zero charge point (pH_{pzc}). The pH value is only used to describe the pH_{pzc} for the systems wherein H^+/OH^- are potentially the determining ions. Mg-Al-HDL pH_{pzc} was measured by the pH drift method [59]. Because of the functional groups such as OH^- , COO^- groups, adsorption of cationic aromatic organics is enhanced at $\text{pH} > \text{pH}_{\text{pzc}}$. In contrast, adsorption of anionic aromatic organics is promoted at $\text{pH} < \text{pH}_{\text{pzc}}$ where the surface is positively charged. As indicated in Figure 5, the pH_{pzc} of Mg-Al-HDL is at 8.01.

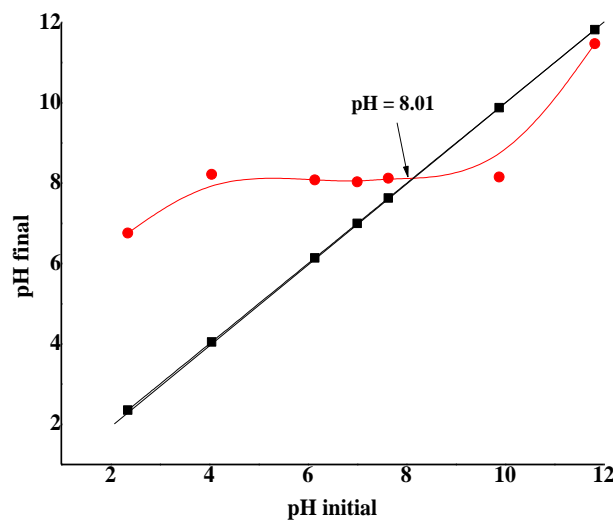


Figure 5. The pH_{PZC} is the point where the plot of final pH versus initial pH corresponds to the intersection of the curve $\text{pH}_{\text{initial}} = \text{pH}_{\text{final}}$ with the bisector axis.

Figure 6 shows that the adsorption is highly dependent on the pH. So, the removal efficiency of GA increased from 38.64 to 56.73 % as the pH value passed from 2 to 7. This behavior may be explained by the zero-point charge of the adsorbent ($pH_{pzc} = 8.01$). At pH values above the zero point charge, the adsorbent surface is negatively charged. It was noted that the removal efficiency is low at $pH < 3$, which indicates that the adsorbed amount decreases. This is explained by the increased protonation of the GA OH groups at $pH < 3$. At this pH range ($pH < pH_{pzc} 8.01$), the surface of the Mg-Al-HDL is positively charged, hence the strong attraction between the Mg-Al-HDL surface and the GA molecule. At $3 < pH_{pzc} < pH$, the yield of removal is enhanced (q_a is decreased), which is explained by the negatively charged surface of Mg-Al-HDL, therefore, a repulsion of the GA molecule. At $pH = pH_{pzc} = 8.01$, the surface of Mg-Al-HDL is neutral, and the molecule of GA is deprotonated. Thus, the attraction between the Mg-Al-HDL surface and the molecule of GA is increased [38].

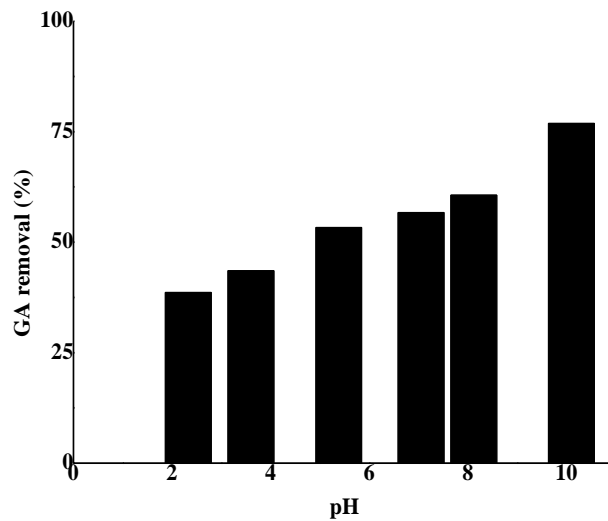


Figure 6. pH effect on the adsorption of GA by Mg-Al-LDH: mass of adsorbent = 0.1 g, $C_0(GA) = 0.1$ mg/L, reaction time = 360 min, $T = 298$ K.

3.2.3. Adsorption kinetic studies.

The effect of contact time on the retention rate is shown in Figure 7 using different initial concentrations of GA. The retention rate increases with the reaction along two different slopes for all used concentrations. The first one is fast within the first 60 min, while the second slope is slow and may express the equilibrium of the adsorbed GA molecules.

The overall retention is comparable for the four concentrations, with decreasing removal efficiencies (0.957, 0.905, 0.673, and 0.56%) as well as increasing adsorbed amounts with values of 24.5, 48.6, 56, and 68.2 mg/g, respectively for concentrations of 25, 50, 80 and 120 mg/L. The main part of the GA transferred to the adsorbent is reached within the first hour with yields of about 0.72, 0.49, 0.35, and 0.29 %, respectively, for the concentrations of 25, 50, 80, and 120 mg/L. The adsorption mechanism and the possible rate control steps required within the adsorption process were investigated using kinetic models such as the intra-particle diffusion, the pseudo-first-order, and the pseudo-second-order models.

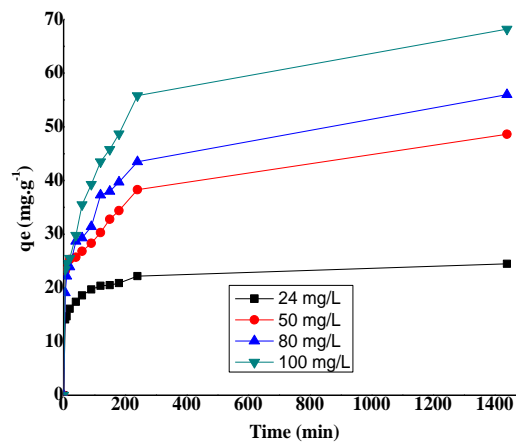


Figure 7. Effect of the contact time on the adsorption of GA in aqueous solution at pH = 4.5 and T = 298 K.

3.2.4. Pseudo-first-order model.

To fit the adsorption kinetic, the non-linear form of the pseudo-first-order model is given using the following equation:

$$q_t = q_e [1 - e^{-(k_1 t)}] \tag{4}$$

where, k_1 represent the pseudo-first-order rate constant (min^{-1}). Results are presented in Figure 8.

Table 3 reports the adsorbed amount values q_e , the pseudo-first-order rate constants k_1 , and the regression coefficients R^2 of the used concentrations. R^2 values are quite low and range from 0.47 to 0.90. The q_e calculation of whole investigated concentrations reveals that the adsorbed amounts of GA are low compared to the experimental q_e . So, it is observed that the GA adsorption is not a controlled diffusion process since it is not in accordance with the pseudo-first-order equation.

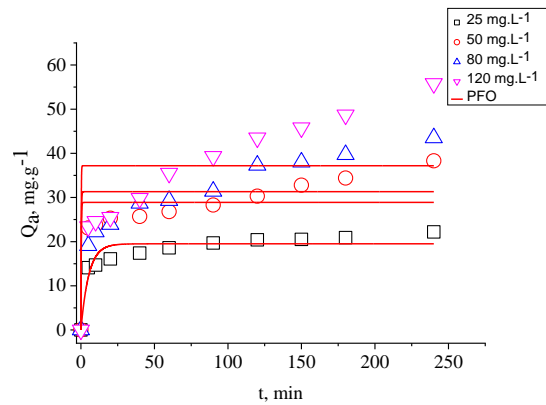


Figure 8. Pseudo-first order kinetic constant for the adsorption of GA onto Mg-Al-LDH.

Table 3: Kinetic parameters for adsorption of GA by Mg-Al-LDH.

C_n mg.L^{-1}	Pseudo-first-order				Pseudo-second-order				Diffusion intra particule			
	K_1 min^{-1}	q_e mg.g^{-1}	R^2	Δq (%)	K_2 $\text{g.mg}^{-1}.\text{min}^{-1}$	q_e mg.g^{-1}	R^2	Δq (%)	k_{id} $\text{mg.g}^{-1}.\text{min}^{-0.5}$	Δq (%)	C	R^2
25	0.18	19.50	0.9027	3.68	0.0144	20.59	0.9597	1.52	5.07	3.87	3.78	0.8978
50	5.20	28.88	0.7471	24.82	0.0102	31.94	0.8754	12.22	8.14	10.60	5.40	0.8920
80	4.96	31.31	0.5540	66.38	0.0028	39.07	0.9029	14.44	10.47	2.24	1.62	0.9849
120	7.67	37.19	0.4716	126.66	0.0014	49.47	0.8575	34.15	13.24	5.60	-0.12	0.9766

3.2.5. Pseudo-second-order model.

The Pseudo-second-order equation may be expressed as [60] K_2 represents the pseudo-second-order rate constant (g/mg.min). The application of the non-linear form of the pseudo-second-order kinetic model (eq 5) to the GA adsorption results is illustrated in Figure 9.

$$q_t = \frac{tk_2q_e^2}{1 + k_2q_e} \tag{5}$$

The adsorbed amount q_{ecal} , the pseudo-second-order rate constants K_2 and the regression coefficients R^2 for the used concentrations are presented in Table 3. Based on the results, the adsorbed amount at equilibrium (q_{ecal}) increases with the initial concentration. Furthermore, the R^2 values significantly exceed those obtained by the pseudo-first-order model. The adsorbed amounts (q_{ecal}) are about 20.59, 31.94, 39.07, and 49.47 mg/g, respectively, for the concentrations of 25, 50, 80, and 120 mg/L and are quite close to the values obtained by the experiments, of about 20.4, 30.30, 37.3, and 43.5 mg/g. These results indicate that the adsorption process is in agreement with the pseudo-second-order model.

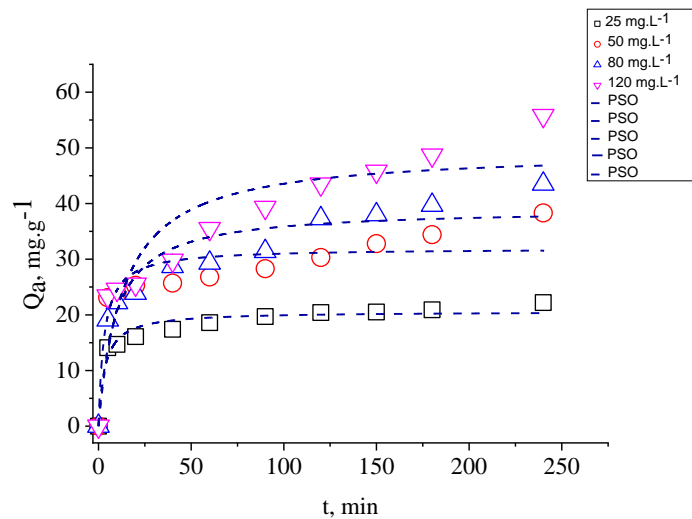


Figure 9. Pseudo-second-order kinetic plot for the adsorption of GA onto Mg-Al-LDH

3.2.6. Intraparticle diffusion model.

Intra-particle diffusion model was examined according to the Weber-Morris theory [61]. Based on this theory, the model may be described as:

$$q_t = k_{id} \cdot t^{1/2} + c \tag{6}$$

where q_t is the adsorbed amount (mg/g) at the time t , and K_{id} is the rate constant for the intraparticle diffusion model ($\text{mg/g} \cdot \text{min}^{1/2}$). The plots of the model for the used GA concentrations are displayed in Figure 10. The intraparticle diffusion rate constant and R^2 is reported in Table 3. It can be observed in Figure 10 that intraparticle diffusion is a relevant step in the GA adsorption process onto Mg-Al-HDL, particularly during the 180 min. This delay can be explained by the migration of GA molecules in the Mg-Al-HDL hydroxalcite sheets. However, the surface chemical reaction that starts within the first few minutes of contact for the experimental data is aligned to the pseudo-second-order with high R^2 regression coefficients, which suggests that the most important step in the GA adsorption onto Mg-Al-HDL is the intraparticle diffusion process since it can be considered as the limiting step that controls the GA transfer at time t .

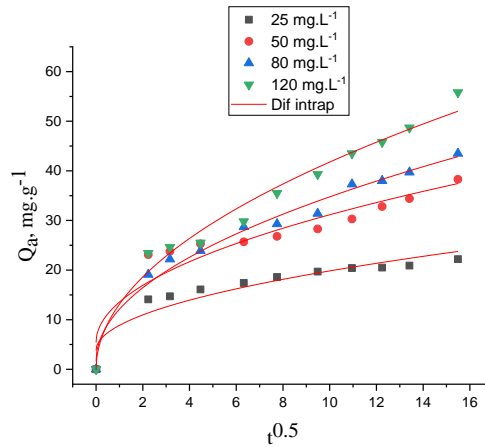


Figure 10. Intraparticle diffusion model for GA adsorption on Mg-Al-LDH

The standard deviation was calculated using the formula (7) to calculate the difference between the curves plotted by the experimental data and the theoretical models. The results are reported in Tables 2 and 3.

$$\Delta q(\%) = \sqrt{\frac{\sum_{i=1}^n (q_{exp} - q_{cal}/q_{exp})^2}{n - 1}} \times 100 \tag{7}$$

with q_{exp} is the adsorbed amount obtained from the experiment, q_{cal} is the adsorbed amount obtained by the theoretical model, and n is the number of experimental points. Based on Table 3, the pseudo-second-order model and the intraparticle diffusion model fit the experimental data well. That is confirmed by the R^2 values that are larger than those of the pseudo-first-order (PFO) model as well as Δq that are small compared to those of the PFO.

3.5. Adsorption mechanism.

In this study, it was shown that the adsorption of GA on hydrotalcite Mg-Al-HDL is pH-dependant, however the adsorption mechanism depends on the pH as well. It is noted that pka of GA is 3.1, when $pH < pka$, the molecule of GA is strongly protonated; therefore, the preponderant form is the anionic form which can be adsorbed on the surface of Mg-Al-HDL through an electrostatic interaction leading to a slight covering of the surface of the LDH favoring in a second step the adsorption of the GA molecule by the forces of π - π and Van der Waals. At $pH > pka$ of phenolic acid, only 20% of the protonated form remained, and these species were adsorbed by coordination bond (complexation) [15].

3.6. Isotherms studies.

Several equation isotherms are used to analyze the experimental sorption equilibrium parameters. The most widely used are the Langmuir and Freundlich models. The Langmuir isotherm model is based on the hypothesis that there are a limited number of homogeneously distributed active sites on the adsorbent surface. Such active sites exhibit a similar affinity for monolayer adsorption, and the adsorbed molecules do not interact [62]. A widely used non-linear form of the Langmuir equation can be expressed as follows [62]:

$$q_e = \frac{q_m K_L C_e}{1 + K_L C_e} \tag{8}$$

where q_e is the adsorbed amount of GA (mg/g), C_e is the concentration at equilibrium (mg/L), as well as q_m and K_L are the Langmuir constants related to the maximal adsorption capacity

(mg/g), and the energy of adsorption (L/mg) [63]. The significant Langmuir isotherm characteristic can be described by a dimensionless factor R_L that is defined as follows [64]:

$$R_L = 1 / (1 + k_L C_0) \tag{9}$$

The value of R_L is used to indicate the process mode of the adsorption isotherm, either if $0 < R_L < 1$ the adsorption is favorable, for $R_L > 1$, the adsorption is unfavorable, for $R_L = 0$ the isotherm is irreversible and linear, for $R_L = 1$. Fitting the experimental data of the adsorption isotherm models, it was noticed that the Langmuir model is the most appropriate to characterize the involved adsorption type. Based on the obtained R_L value, it can be concluded that the process is favorable $R_L = 0.101, 0.053, 0.033, 0.022$ ($0 < R_L < 1$). Hence, the GA molecules can be adsorbed in a monolayer without any interaction GA-GA.

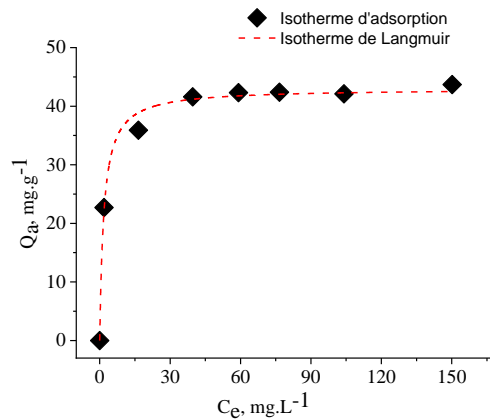


Figure12. Langmuir isotherm for the adsorption of GA onto Mg-Al-LDH.

Freundlich adsorption isotherm model is applied to heterogeneous surface adsorption with adsorbed molecules interaction, and it is not limited to forming a monolayer. It is assumed that with the increasing concentration of the adsorbate, the adsorbate concentration at the surface of the adsorbent is also increasing. Therefore, the adsorption energy is exponentially decreased at the end of the sorption of the adsorbent. The expression of the non-linear Freundlich model is given as [65]:

$$q_e = K_F C_e^{1/n_F} \tag{10}$$

The equilibrium adsorbed amount is q_e (mg/g), K_F is the Freundlich constant, $1/n_F$ is the heterogeneity factor related to the adsorption capacity and intensity, and C_e is the concentration at equilibrium (mg/L).

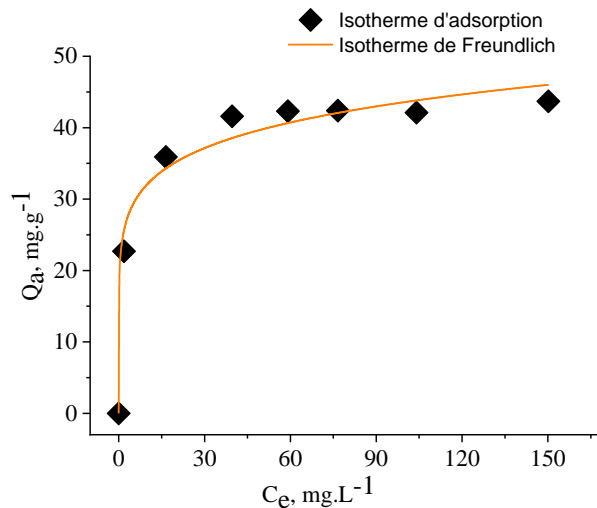


Figure 13. Freundlich isotherms for the adsorption of GA onto Mg-Al-LDH.

It is noticed in Table 3 that the Langmuir model is in accord with the experimental results and that by comparing the values of R^2 , which is close to 1 and the lower Δq than that of the Freundlich model.

4. Conclusions

In the present study, the Mg-Al-LDH hydrotalcite was synthesized through the co-precipitation method for the degradation of GA. The parameters of initial GA concentration, contact time, and temperature revealed a significant effect on the GA removal by Mg-Al-LDH from aqueous solutions. The Langmuir and Freundlich isotherm models were used to describe the adsorption equilibrium of GA on Mg-Al-LDH mathematically. The Langmuir isotherm model was shown to be the most appropriate model to fit the experimental data in the investigated temperature range. The kinetic adsorption results demonstrated that the adsorption process followed the pseudo-second-order model. Thermodynamic results indicated the feasibility, endothermic, and spontaneous nature of the adsorption process involved at 18 - 38°C. The various obtained results indicated that the adsorbent selected in this study was efficient and suitable for removing GA and industrial effluents.

Funding

This research received no external funding.

Acknowledgments

This work is supported by the Directorate General for Scientific Research and Technological Development DGRSDT.

Conflicts of Interest

The authors declare no conflict of interest.

References

1. Hodgson, J.M.; Morton, L.W.; Puddey, I.B.; Beilin, L.J.; Croft, K.D. Gallic Acid Metabolites Are Markers of Black Tea Intake in Humans. *J. Agric. Food Chem.* **2000**, *48*, 2276-2280, <https://doi.org/10.1021/jf000089s>.
2. Schulz, H.; Albroseheit, G. High-performance liquid chromatographic characterization of some medical plant extracts used in cosmetic formulas. *J. Chromatogr. A* **1988**, *442*, 353-361, [https://doi.org/10.1016/s0021-9673\(00\)94483-2](https://doi.org/10.1016/s0021-9673(00)94483-2).
3. Shahmirifard, S.A.; Ghaedi, M.; Razmi, Z.; Hajati, S. A simple ultrasensitive electrochemical sensor for simultaneous determination of gallic acid and uric acid in human urine and fruit juices based on zirconia-choline chloride-gold nanoparticles-modified carbon paste electrode. *Biosens. Bioelectron.* **2018**, *114*, 30-36, <https://doi.org/10.1016/j.bios.2018.05.009>.
4. Bahrani, S.; Ghaedi, M.; Daneshfar, A. Fabrication of size controlled nanocomposite based on zirconium alkoxide for enrichment of Gallic acid in biological and herbal tea samples. *J. Chromatogr. B* **2018**, *1087-1088*, 14-22. <https://doi.org/10.1016/j.jchromb.2018.1004.1021>.
5. Vilian, A.T.E.; Song, J.Y.; Lee, Y.S.; Hwang, S.-K.; Kim, H.J.; Jun, Y.-S.; Huh, Y.S.; Han, Y.-K. Salt-templated three-dimensional porous carbon for electrochemical determination of gallic acid. *Biosens. Bioelectron.* **2018**, *117*, 597-604. <https://doi.org/10.1016/j.bios.2018.06.064>.
6. Zaldivar, J.; Ingram, L.O. Effect of organic acids on the growth and fermentation of ethanologenic *Escherichia coli* LY01. *Biotechnol. Bioeng.* **1999**, *66*, 203-210, <https://pubmed.ncbi.nlm.nih.gov/10578090/>.
7. Fiuza, S.M.; Gomes, C.; Teixeira, L.J.; Girão da Cruz, M.T.; Cordeiro, M.N.D.S.; Milhazes, N.; Borges, F.; Marques, M.P.M. Phenolic acid derivatives with potential anticancer properties—a structure–activity

- relationship study. Part 1: Methyl, propyl and octyl esters of caffeic and gallic acids. *Bioorg. Med. Chem.* **2004**, *12*, 3581-3589, <https://pubmed.ncbi.nlm.nih.gov/15186842/>.
8. Wu, Y.; Zhou, K.; Dong, S.; Yu, W.; Zhang, H. Recovery of gallic acid from gallic acid processing wastewater. *Environ. Technol.* **2015**, *36*, 661-666, <https://pubmed.ncbi.nlm.nih.gov/25249197/>.
 9. Víctor-Ortega, M.D.; Airado-Rodríguez, D. Revalorization of agro-industrial effluents based on gallic acid recovery through a novel anionic resin. *Process Saf. Environ. Prot* **2018**, *115*, 17-26, <https://www.sciencedirect.com/science/article/pii/S0957582017302604>.
 10. Zhang, Z.; Pang, Q.; Li, M.; Zheng, H.; Chen, H.; Chen, K. Optimization of the condition for adsorption of gallic acid by *Aspergillus oryzae* mycelia using Box-Behnken design. *Environ. Sci. Pollut. Res.* **2015**, *22*, 1085-1094, <https://doi.org/10.1007/s11356-014-3409-3>.
 11. Lu, L.-L.; Lu, X.-Y. Solubilities of Gallic Acid and Its Esters in Water. *J. Chem. Eng. Data* **2007**, *52*, 37-39., <https://pubs.acs.org/doi/10.1021/je0601661>.
 12. Benitez, F.J.; Real, F.J.; Acero, J.L.; Leal, A.I.; Garcia, C. Gallic acid degradation in aqueous solutions by UV/H₂O₂ treatment, Fenton's reagent and the photo-Fenton system. *J. Hazard. Mater.* **2005**, *126*, 31-39, <https://doi.org/10.1016/j.jhazmat.2005.04.040>.
 13. Saldaña-Flores, K.E.; Flores-Estrella, R.A.; Alcaraz-Gonzalez, V.; Carissimi, E.; de Souza, B.G.; Ruotolo, L.A.M.; Urquieta-Gonzalez, E. Regulation of Hydrogen Peroxide Dosage in a Heterogeneous Photo-Fenton Process. *Processes* **2021**, *9*, 2167, <http://dx.doi.org/10.3390/pr9122167>.
 14. Chedri Mammam, A.; Mouni, L.; Bollinger, J.-C.; Belkhir, L.; Bouzaza, A.; Assadi, A.A.; Belkacemi, H. Modeling and optimization of process parameters in elucidating the adsorption mechanism of Gallic acid on activated carbon prepared from date stones. *Sep. Sci. Technol* **2020**, *55*, 3113-3125, <https://www.tandfonline.com/doi/abs/10.1080/01496395.2019.1676785>.
 15. Ahmat, A.M.; Thiebault, T.; Guégan, R. Phenolic acids interactions with clay minerals: A spotlight on the adsorption mechanisms of Gallic Acid onto montmorillonite. *Appl. Clay Sci.* **2019**, *180*, 105188. <https://doi.org/10.1016/j.clay.2019.105188>.
 16. Li, J.; Zhou, X.; Yan, Y.; Shen, D.; Lu, D.; Guo, Y.; Xie, L.; Deng, B. Selective Recognition of Gallic Acid Using Hollow Magnetic Molecularly Imprinted Polymers with Double Imprinting Surfaces. *Polymers* **2022**, *14*, 175, <https://doi.org/10.3390/polym14010175>.
 17. Gadiri, A.; Benkhaled, A.; Choukchou-Braham, E. Equilibrium, kinetic and thermodynamic studies of copper adsorption onto poly(n-vinylpyrrolidone) modified clay. *J. Macromol. Sci. A* **2018**, *55*, 393-400, <https://www.tandfonline.com/doi/abs/10.1080/10601325.2018.1453258>.
 18. Zazoua, H.; Boudjemaa, A.; Chebout, R.; Bachari, K. Enhanced photocatalytic hydrogen production under visible light over a material based on magnesium ferrite derived from layered double hydroxides (LDHs). *Int. J. Energy Res* **2014**, *38*, 2010-2018, <https://onlinelibrary.wiley.com/doi/abs/10.1002/er.3215>.
 19. Zhang, W.; Dong, T.; Cheng, H.; Wu, H.; Wu, C.; Hu, A.; Wang, D. Preparation of composite sludge carbon-based materials by LDHs conditioning and carbonization and its application in the simultaneous removal of dissolved organic matter and phosphate in sewage. *Chemosphere* **2021**, *270*, 129485, <https://doi.org/10.1016/j.chemosphere.2020.129485>.
 20. Goh, K.-H.; Lim, T.-T.; Dong, Z. Application of layered double hydroxides for removal of oxyanions: A review. *Water Res.* **2008**, *42*, 1343-1368. <https://doi.org/10.1016/j.watres.2007.10.043>.
 21. Das, D.P.; Das, J.; Parida, K. Physicochemical characterization and adsorption behavior of calcined Zn/Al hydrotalcite-like compound (HTlc) towards removal of fluoride from aqueous solution. *J. Colloid Interface Sci.* **2003**, *261*, 213-220, <https://pubmed.ncbi.nlm.nih.gov/16256525/>.
 22. Cosano, D.; Esquivel, D.; Romero-Salguero, F.J.; Jiménez-Sanchidrián, C.; Ruiz, J.R. Efficient Removal of Nonylphenol Isomers from Water by Use of Organo-Hydrotalcites. *Int. J. Environ. Res. Public Health* **2022**, *19*, 7214, <https://pubmed.ncbi.nlm.nih.gov/35742463/>.
 23. Tang, Y.; Slay, M.; Yang, Y.; Li, S.; Qin, F.; Zhao, Y.; Zhang, Z.; Zhang, L. Highly active Mg-Al hydrotalcite for efficient O-methylation of phenol with DMC based on soft colloidal templates. *J. Chem. Technol. Biotechnol.* **2022**, *97*, 79-86, <https://onlinelibrary.wiley.com/doi/abs/10.1002/jctb.6912>.
 24. Devesa-Rey, R.; del Val, J.; Feijoo, J.; González-Coma, J.P.; Castiñeira, G.; González-Gil, L. Preparation of Synthetic Clays to Remove Phosphates and Ibuprofen in Water. *Water* **2021**, *13*, 2394, <https://doi.org/10.3390/w13172394>.
 25. Das, J.; Patra, B.S.; Baliarsingh, N.; Parida, K.M. Adsorption of phosphate by layered double hydroxides in aqueous solutions. *Appl. Clay Sci.* **2006**, *32*, 252-260, <https://doi.org/10.1016/j.clay.2006.02.005>.
 26. Peng, S.; Lü, L.; Wang, J.; Han, L.; Chen, T.; Jiang, S. Study on the adsorption kinetics of orthophosphate anions on layer double hydroxide. *Chin. J. Geochem.* **2009**, *28*, 184-187, <https://link.springer.com/article/10.1007/s11631-009-0184-9>.
 27. Lv, L.; He, J.; Wei, M.; Evans, D.G.; Zhou, Z. Treatment of high fluoride concentration water by MgAl-CO₃ layered double hydroxides: Kinetic and equilibrium studies. *Water Res.* **2007**, *41*, 1534-1542, <https://doi.org/10.1016/j.watres.2006.12.033>.
 28. Grover, K.; Komarneni, S.; Katsuki, H. Synthetic hydrotalcite-type and hydrocalumite-type layered double hydroxides for arsenate uptake. *Appl. Clay Sci.* **2010**, *48*, 631-637, <https://doi.org/10.1016/j.clay.2010.03.017>.

29. Grover, K.; Komarneni, S.; Katsuki, H. Uptake of arsenite by synthetic layered double hydroxides. *Water Res.* **2009**, *43*, 3884-3890, <https://doi.org/10.1016/j.watres.2009.06.003>.
30. Prasanna, S.V.; Rao, R.A.P.; Kamath, P.V. Layered double hydroxides as potential chromate scavengers. *J. Colloid Interface Sci.* **2006**, *304*, 292-299, <https://doi.org/10.1016/j.jcis.2006.08.064>.
31. You, Y.; Vance, G.F.; Zhao, H. Selenium adsorption on Mg–Al and Zn–Al layered double hydroxides. *Appl. Clay Sci.* **2001**, *20*, 13-25, [https://doi.org/10.1016/S0169-1317\(00\)00043-0](https://doi.org/10.1016/S0169-1317(00)00043-0).
32. Halajnia, A.; Oustan, S.; Najafi, N.; Khataee, A.R.; Lakzian, A. The adsorption characteristics of nitrate on Mg–Fe and Mg–Al layered double hydroxides in a simulated soil solution. *Appl. Clay Sci.* **2012**, *70*, 28-36, <https://doi.org/10.1016/j.clay.2012.09.007>.
33. Sasai, R.; Fujimura, T.; Sato, H.; Nii, E.; Sugata, M.; Nakayashiki, Y.; Hoashi, H.; Moriyoshi, C.; Oishi, E.; Fujii, Y.; et al. Origin of Selective Nitrate Removal by Ni²⁺–Al³⁺ Layered Double Hydroxides in Aqueous Media and Its Application Potential in Seawater Purification. *Bull. Chem. Soc. Jap.* **2022**, *95*, 802-812, <https://www.journal.csj.jp/doi/full/10.1246/bcsj.20220032>.
34. Liu, X.; Lu, S.; Tang, Z.; Wang, Z.; Huang, T. Removal of sulfate from aqueous solution using Mg–Al nano-layered double hydroxides synthesized under different dual solvent systems. *Nanotechnol. Rev.* **2021**, *10*, 117-125, <https://www.degruyter.com/document/doi/10.1515/ntrev-2021-0012/html?lang=en>.
35. Lv, L.; He, J.; Wei, M.; Evans, D.G.; Duan, X. Uptake of chloride ion from aqueous solution by calcined layered double hydroxides: Equilibrium and kinetic studies. *Water Res.* **2006**, *40*, 735-743, <https://doi.org/10.1016/j.watres.2005.11.043>.
36. Kim, G.; Park, S. Chloride Removal of Calcium Aluminate-Layered Double Hydroxide Phases: A Review. *Int. J. Environ. Res. Public Health* . **2021**, *18*, 2797, <https://www.ncbi.nlm.nih.gov/pmc/articles/PMC7999922/>.
37. Gillman, G.P. A simple technology for arsenic removal from drinking water using hydrotalcite. *Sci. Total Environ.* **2006**, *366*, 926-931, <https://pubmed.ncbi.nlm.nih.gov/16546240/>.
38. Santosa, S.J.; Fitriani, D.; Aprilita, N.H.; Rusdiarso, B. Gallic and salicylic acid-functionalized Mg/Al hydrotalcite as highly effective materials for reductive adsorption of AuCl₄⁻. *Appl. Surf. Sci.* **2020**, *507*, 145115, <https://doi.org/10.1016/j.apsusc.2019.145115>.
39. Cai, L.; Zhang, Y.; Peng, X.; Guo, F.; Ji, L.; Li, L. Preparation of layered double hydroxide intercalated by Gallic acid for boron adsorption. *J. Water Process. Eng.* **2021**, *44*, 102394, <https://doi.org/10.1016/j.jwpe.2021.102394>.
40. Genovese, S.; Epifano, F.; Marchetti, L.; Bastianini, M.; Cardellini, F.; Spogli, R.; Fiorito, S. Pre-concentration of active principles from different varieties of *Camellia sinensis* extracts by solid sorbents. *J. Pharm. Biomed. Anal.* **2021**, *196*, 113945, <https://doi.org/10.1016/j.jpba.2021.113945>.
41. Taoufik, N.; Boumya, W.; Elhalil, A.; Achak, M.; Sadiq, M.; Abdennouri, M.; Barka, N. Gallic acid removal using fresh and calcined Ni-Al layered double hydroxides: Kinetics, equilibrium and response surface methodology (RSM) optimisation. *J. Environ. Anal. Chem.* **2021**, 1-25, <https://doi.org/10.1080/03067319.2020.1863387>.
42. Badhani, B.; Sharma, N.; Kakkar, R. Gallic acid: a versatile antioxidant with promising therapeutic and industrial applications. *RSC Adv.* **2015**, *5*, 27540-27557, <https://pubs.rsc.org/en/content/articlelanding/2015/ra/c5ra01911g>.
43. Dhiman, S.; Mukherjee, G. Gallic Acid (GA): A Multifaceted Biomolecule Transmuting the Biotechnology Era. In *Recent Developments in Microbial Technologies*, Prasad, R., Kumar, V., Singh, J., Upadhyaya, C.P., Eds.; Springer Nature Singapore: Singapore, **2021**; 163-202, https://link.springer.com/chapter/10.1007/978-981-15-4439-2_8.
44. Alfei, S.; Oliveri, P.; Malegori, C. Assessment of the Efficiency of a Nanospherical Gallic Acid Dendrimer for Long-Term Preservation of Essential Oils: An Integrated Chemometric-Assisted FTIR Study. *ChemistrySelect* **2019**, *4*, 8891-8901, <https://chemistry-europe.onlinelibrary.wiley.com/doi/abs/10.1002/slct.201902339>.
45. Fereidoonfar, H.; Salehi-Arjmand, H.; Khadivi, A.; Akramian, M.; Safdari, L. Chemical variation and antioxidant capacity of sumac (*Rhus coriaria* L.). *Ind. Crops Prod.* **2019**, *139*, 111518, <https://doi.org/10.1016/j.indcrop.2019.111518>.
46. Zhao, J.; Khan, I.A.; Fronczek, F.R. Gallic acid. *Acta Crystallographica Section E* **2011**, *67*, o316-o317, <https://doi.org/10.1107/S1600536811000262>.
47. Damiani, E.; Bacchetti, T.; Padella, L.; Tiano, L.; Carloni, P. Antioxidant activity of different white teas: Comparison of hot and cold tea infusions. *J. Food Compos. Anal.* **2014**, *33*, 59-66, <https://doi.org/10.1016/j.jfca.2013.09.010>.
48. Reichle, W.T. Catalytic reactions by thermally activated, synthetic, anionic clay minerals. *J. Catal.* **1985**, *94*, 547-557, [https://doi.org/10.1016/0021-9517\(85\)90219-2](https://doi.org/10.1016/0021-9517(85)90219-2).
49. Kerchich, S.; Boudjemaa, A.; Chebout, R.; Bachari, K.; Mameri, N. High performance of δ-Fe₂O₃ novel photo-catalyst supported on LDH structure. *J. Photochem. Photobiol.* **2021**, *406*, 113001, <https://doi.org/10.1016/j.jphotochem.2020.113001>.
50. Cavani, F.; Trifirò, F.; Vaccari, A. Hydrotalcite-type anionic clays: Preparation, properties and applications. *Catal. Today.* **1991**, *11*, 173-301, [https://doi.org/10.1016/0920-5861\(91\)80068-K](https://doi.org/10.1016/0920-5861(91)80068-K).

51. Obijole, O.; Muger, G.W.; Mudzielwana, R.; Ndungu, P.; Samie, A.; Babatunde, A. Hydrothermally treated aluminosilicate clay (HTAC) for remediation of fluoride and pathogens from water: Adsorbent characterization and adsorption modelling. *Water Resour. Ind.* **2021**, *25*, 100144, <https://doi.org/10.1016/j.wri.2021.100144>.
52. Xie, X.; Yan, K.; Li, J.; Wang, Z. Efficient synthesis of benzoin methyl ether catalyzed by hydrotalcite containing cobalt. *Catal. Commun.* **2008**, *9*, 1128-1131, <https://doi.org/10.1016/j.catcom.2007.10.020>.
53. Carriazo, D.; del Arco, M.; Martín, C.; Rives, V. A comparative study between chloride and calcined carbonate hydrotalcites as adsorbents for Cr(VI). *Appl. Clay Sci.* **2007**, *37*, 231-239, <https://doi.org/10.1016/j.clay.2007.01.006>.
54. Frost, R.L.; Spratt, H.J.; Palmer, S.J. Infrared and near-infrared spectroscopic study of synthetic hydrotalcites with variable divalent/trivalent cationic ratios. *Spectrochim. Acta - A: Mol. Biomol.* **2009**, *72*, 984-988, <https://doi.org/10.1016/j.saa.2008.12.018>.
55. Bouraada, M.; Lafjah, M.; Ouali, M.S.; de Menorval, L.C. Basic dye removal from aqueous solutions by dodecylsulfate- and dodecyl benzene sulfonate-intercalated hydrotalcite. *J. Hazard. Mater.* **2008**, *153*, 911-918, <https://doi.org/10.1016/j.jhazmat.2007.09.076>.
56. Yu, X.; Wang, J.; Zhang, M.; Yang, P.; Yang, L.; Cao, D.; Li, J. One-step synthesis of lamellar molybdate pillared hydrotalcite and its application for AZ31 Mg alloy protection. *Solid State Sci.* **2009**, *11*, 376-381, <https://doi.org/10.1016/j.solidstatesciences.2008.08.003>.
57. Yu, Z.; Chen, D.; Rønning, M.; Vrålstad, T.; Ochoa-Fernández, E.; Holmen, A. Large-scale synthesis of carbon nanofibers on Ni-Fe-Al hydrotalcite derived catalysts: I. Preparation and characterization of the Ni-Fe-Al hydrotalcites and their derived catalysts. *Appl Catal A Gen.* **2008**, *338*, 136-146, <https://doi.org/10.1016/j.apcata.2008.01.003>.
58. Li, F.; Jiang, X.; Evans, D.G.; Duan, X. Structure and Basicity of Mesoporous Materials from Mg/Al/In Layered Double Hydroxides Prepared by Separate Nucleation and Aging Steps Method. *J. Porous Mater.* **2005**, *12*, 55-63, <https://link.springer.com/article/10.1007/s10934-005-5234-z>.
59. Doğan, M.; Alkan, M.; Çakir, Ü. Electrokinetic Properties of Perlite. *J. Colloid Interface Sci.* **1997**, *192*, 114-118, <https://doi.org/10.1006/jcis.1997.4913>.
60. Ho, Y.S.; McKay, G. Pseudo-second order model for sorption processes. *Process Biochem* **1999**, *34*, 451-465, [https://doi.org/10.1016/S0032-9592\(98\)00112-5](https://doi.org/10.1016/S0032-9592(98)00112-5).
61. Weber, W.J.; Morris, J.C. Kinetics of Adsorption on Carbon from Solution. *J. Sanit. Eng. Div.* **1963**, *89*, 31-59, <https://ascelibrary.org/doi/abs/10.1061/JSEDAI.0000430>.
62. Langmuir, I. THE ADSORPTION OF GASES ON PLANE SURFACES OF GLASS, MICA AND PLATINUM. *J. Am. Chem. Soc.* **1918**, *40*, 1361-1403, <https://doi.org/10.1021/ja02242a004>.
63. Doğan, M.; Alkan, M. Removal of methyl violet from aqueous solution by perlite. *J. Colloid Interface Sci.* **2003**, *267*, 32-41, [https://doi.org/10.1016/S0021-9797\(03\)00579-4](https://doi.org/10.1016/S0021-9797(03)00579-4).
64. Weber, T.W.; Chakravorti, R.K. Pore and solid diffusion models for fixed-bed adsorbents. *AIChE J* **1974**, *20*, 228-238, <https://aiche.onlinelibrary.wiley.com/doi/10.1002/aic.690200204>.
65. Clayton, W. Capillary and colloid chemistry. By Prof. H. Freundlich. Translated by H. Stafford Hatfield, B.Sc., Ph.D. pp. xv+883. London: Methuen and Co., Ltd., 1926. Price: 50s. *J.Soc.Chem Ind.* **1926**, *45*, 797-798, <https://doi.org/10.1002/jctb.5000454407>.